PHYSICAL REVIEW B **90**, 205201 (2014)

Experimental versus *ab initio* x-ray absorption of iron-doped zirconia: Trends in O K-edge spectra as a function of iron doping

D. H. Douma,[1] R. Ciprian,[2] A. Lamperti,[1] P. Lupo,[3] E. Cianci,[1] D. Sangalli,[1] F. Casoli,[3] L. Nasi,[3] F. Albertini,[3]
P. Torelli,[2] and A. Debernardi[1]
[1]*Laboratorio MDM, IMM-CNR, via C. Olivetti 2, 20864 Agrate Brianza (MB), Italy*
[2]*Laboratorio TASC, IOM-CNR, S.S. 14 km 163.5, Basovizza, I-34149 Trieste, Italy*
[3]*CNR-IMEM, Parco Area delle Scienze 37/A, 43124 Parma (PR), Italy*

(Received 17 July 2014; revised manuscript received 9 September 2014; published 4 November 2014)

We present an experimental study of x-ray absorption near edge structure (XANES) at $L_{2,3}$, $M_{2,3}$, and K edges of, respectively, Fe, Zr, and O in iron-doped zirconia (ZrO_2:Fe) for different Fe dopant concentrations x (from $x \sim 6\%$ to $x \sim 25\%$ at.) and make the comparison with *ab initio* simulations at the O K-edge. The x-ray magnetic circular dichroism (XMCD) measurements show no evidence of ferromagnetic (FM) order for all the analyzed samples in agreement with our *ab initio* simulations, which show an antiferromagnetic (AFM) order. We found that substituting Zr with Fe atoms leads to a radical change in the O K-edge XANES spectrum, especially in the pre-edge region where a pre-edge peak appears. This pre-edge peak is ascribed to dipole transitions from O 1s to O 2p states that are hybridized with the unoccupied Fe 3d states. Both theoretical and experimental results reveal that the intensity of the pre-edge peak increases with Fe concentration, suggesting the increase of unoccupied Fe 3d states. The increase of Fe concentration increases oxygen vacancies as required for charge neutrality and consequently improves AFM ordering. According to our first-principles calculations, the effect of one Fe atom is mostly localized in the first oxygen shell and vanishes as one moves far from it. Thus the increase of the O K-pre-edge peak with increasing Fe concentration is due to the increase of percentage of oxygen atoms that are near neighbors to Fe atoms.

DOI: 10.1103/PhysRevB.90.205201 PACS number(s): 61.05.cj, 75.50.Pp, 68.55.Ln, 71.15.Mb

I. INTRODUCTION

Spintronics is a branch of research that exploits the charge and spin of an electron for carrying and storing information. In the near future, spintronics technology will lead to a fundamental transformation of current electronic devices such as computer's memories, permitting much faster operations, low-energy consumption, and their extreme miniaturization. This miniaturization requires the development of new materials insensitive to parasitic external magnetic fields, while preserving the magnetoresistive signals of existing systems based on giant or tunnel magnetoresistance [1]. This could be obtained in tunnel anisotropic magnetoresistance structures incorporating antiferromagnetic (AFM) materials instead of ferromagnetic (FM) ones [1], opening a route towards AFM spintronics [2].

In recent years, diluted magnetic semiconductors (DMS) and diluted magnetic oxides (DMO) have attracted great attention due to their potential applications in spintronics devices. In such materials, a room temperature magnetism is generated by introducing a certain concentration of magnetic ions such as transition metals. Recently, Nguyen *et al.* [3] reported the existence of ground state antiferromagnetic order in iron-doped zirconia (ZrO_2:Fe) films at diluted concentration ($x = 6.25\%$), from *ab initio* electronic structure calculations and experimental investigations, where the samples were prepared by pulsed laser deposition (PLD) technique. By fitting the magnetization data to Curie Weiss law, Yu *et al.* [4] also reported the presence of AFM order in nanoparticles of ZrO_2:Fe prepared by a coprecipitation method, and its enhancement with the increase of Fe concentration (from $x = 15\%$ up to 40%). However, the mechanism responsible for the enhancement of magnetic properties with the increase of dopant concentration is still lacking.

In the present work, we explore the structural and electronic properties of ZrO_2:Fe for different Fe atomic concentrations x (from $x \sim 6\%$ up to $\sim 25\%$). We used x-ray absorption near-edge structure (XANES) spectroscopy, both experimentally and theoretically, to elucidate the magnetic ordering and its enhancement with the increase of Fe dopant concentration in this DMO.

This paper is organized as follow. In Sec. II, we give an overview of experimental framework and present the experimental XANES spectra at the $L_{2,3}$, $M_{2,3}$, and K edges of, respectively, Fe, Zr, and O. In Sec. III, we detail the theoretical framework, compare the experimental and theoretical XANES spectra at the O K-edge with respect to the increase of Fe dopant concentration and interpret their features in the pre-edge region using local density of states (DOS). The conclusion is given in Sec. IV.

II. EXPERIMENTAL APPROACH

A. Experimental technique

Experimentally ZrO_2 and ZrO_2:Fe thin films were grown on Si/SiO_2 substrates in a flow-type hot wall atomic layer deposition reactor (ASM F120) starting from β-diketonates metalorganic precursors, namely Zr(TMHD)$_4$ for Zr and Fe(TMHD)$_3$ for Fe (TMHD = 2, 2, 6, 6-tetramethyl-3, 5-heptanedionate). To grant a stable reactivity, Zr precursor was kept at 170 °C, while Fe precursor was maintained at 115 °C. Ozone was used as oxidizing gas in the reaction process. The film growth was achieved by alternately introducing the reactants separated by N_2 inert gas purging pulses. The growth temperature was maintained at 350 °C and the Fe concentration in ZrO_2:Fe films was tuned tailoring the Zr/Fe precursors pulsing ratio. After the deposition, the films were annealed at 800 °C in N_2 flux for 60 s. Film thickness was monitored by spectroscopic ellipsometry (SE) (Woollam M-2000 F) and further calculated, along with surface roughness and electron density, by specular x-ray reflectivity (XRR) (Italstructure XRD 3000). Film crystallinity was checked by x-ray diffraction (XRD) at fixed grazing incidence angle $\omega = 1^\circ$ and using a CuK_α ($\lambda = 0.154$ nm) monochromated and collimated x-ray beam. The film uniform doping along its thickness was checked by time of flight secondary ion mass spectrometry (ToF-SIMS) depth profiling using an ION-TOF IV instrument, with 500 eV Cs^+ ions for sputtering and 25 keV Ga^+ ions for analysis. Secondary ions were collected in negative polarity and interlaced mode. The recorded intensities were normalized to the ^{30}Si intensity in bulk silicon. In these operating conditions, the instrument depth resolution is below 1 nm. The details of the growth process and the results of the above mentioned characterization are identical to those we have reported in our previous works [5–8].

To elucidate the Fe chemical state and concentration in $\mathrm{ZrO_2}$:Fe films, x-ray photoemission (XPS) measurements were performed on a PHI 5600 instrument equipped with a monochromatic Al K_α x-ray source ($E = 1486.6$ eV) and a concentric hemispherical analyzer. The spectra were collected at a take-off angle of 45° and band-pass energy 11.50 eV. The instrument resolution is 0.5 eV. X-ray absorption spectroscopy (XAS) and x-ray magnetic circular dichroism (XMCD) at the $L_{2,3}$, $M_{2,3}$, and K edges of, respectively, Fe, Zr, and O, were performed at room temperature (RT) and at 30 K at APE Beamline of the Elettra synchrotron (Trieste, Italy) [9]. The spectra were acquired in total electron yield (TEY) mode by recording the drain current, the light was circularly polarized with 75% of polarization degree, and the beam was impinging at 45° with respect to the surface normal. The XMCD spectra were measured (i) on samples in their remanence state after applying a pulsed in-plane magnetic field of about 500 Oe, (ii) applying a static in-plane magnetic field of about 200 Oe, and (iii) after a field cooling treatment in an applied in-plane field of almost 100 Oe. The magnetization direction was reversed at each point of the XMCD/XAS spectra. Moreover, in order to avoid possible field asymmetries and systematic errors, the spectra were measured with opposite photon helicities. The photon energy resolution was 60 meV for the Zr $M_{2,3}$-edge, 100 meV for the O K-edge, and 130 meV for the Fe $L_{2,3}$-edge.

B. Experimental results

In this experiment, we measured XAS and XMCD spectra of $\mathrm{ZrO_2}$ thin films doped with different Fe atomic concentrations namely $x = 6\%$, 11%, 15%, 20%, and 24%. The XAS spectra at the $M_{2,3}$, K, and $L_{2,3}$ edges of Zr, O, and Fe, respectively, for the analyzed samples are reported in Fig. 1.

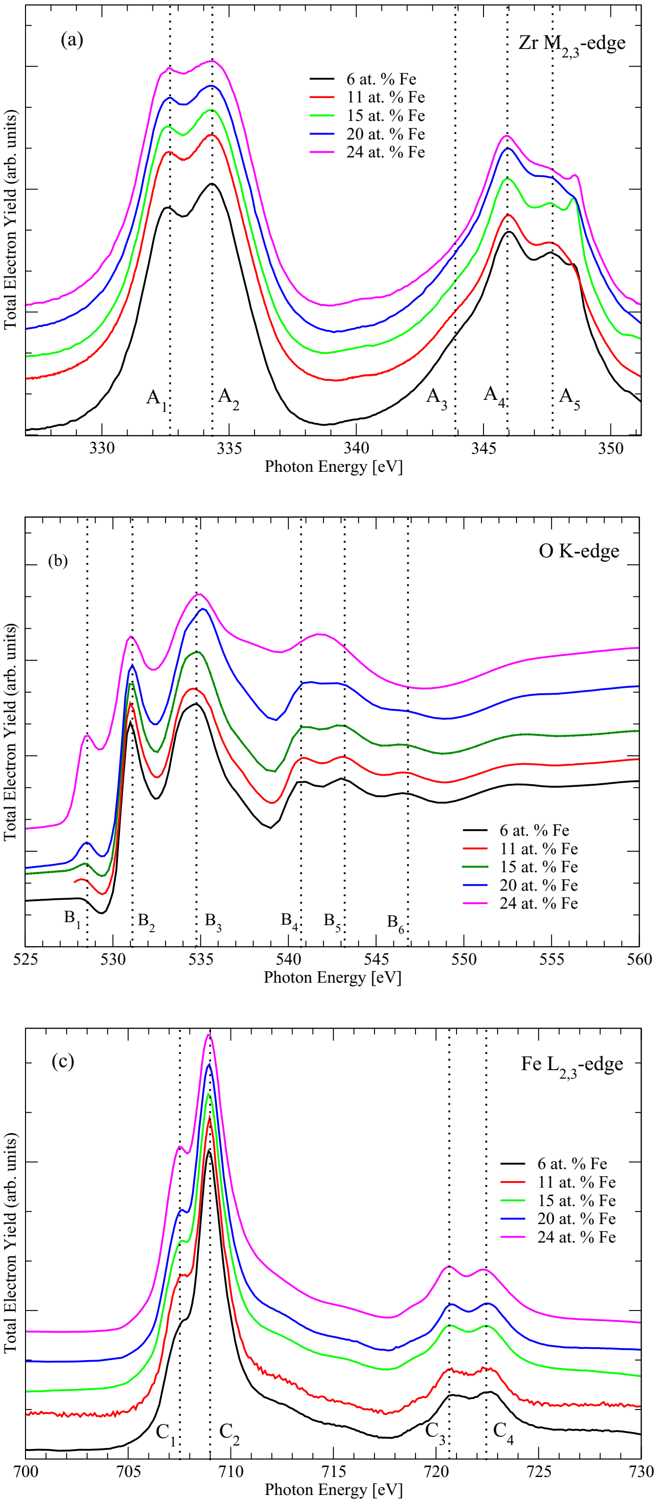

FIG. 1. (Color online) Room temperature XAS spectra recorded in TEY mode for the different Fe-doped samples: (a) Zr $M_{2,3}$, (b) O K, and (c) Fe $L_{2,3}$ edges.

The Zr $3p$ edge XAS [Fig. 1(a)] of the films shows two strong multicomponent bands. The features can be assigned to the transitions from the Zr $3p$ to the states $4d$ (332–334 and 346–348 eV marked with $A_{1,2}$ and $A_{4,5}$ in the figure) and $5s$ (shoulder at 344 eV, marked with A_3) [10]. The relative intensities of the first subpeaks at A_1 and A_2 suggest that the samples show mainly the tetragonal structure [11]. However, only the samples doped with the concentrations $x = 6\%$, 11%, and 15% of Fe show a clear shoulder A_3 indicating that the films with Fe atomic concentration higher than 15% contain a relatively large amount of the cubic/monoclinic phase.

Figure 1(b) shows the corresponding spectra of the O K-edge. It is to point out that the incident photon flux I_0 was measured on a grid placed at the experimental chamber which was not free from oxygen contamination. However, the acquired TEY signals are in very good agreement with those normally reported in literature for oxygen [12–15]. Moreover, the acquired I_0 is not responsible for the relative variations in the spectra giving us a good confidence for a qualitative interpretation of the results. The O K-edge spectra can be divided into two regions. In the energy range 530–534 eV (B_2 and B_3) the peaks are due to transitions from O 1s to O 2p state hybridized with the Zr 4d states [16]. The well resolved shape of these peaks suggests that the samples are crystalline, moreover, the higher energy peak B_3 is very broad in agreement with the presence of a well ordered tetragonal structure [11,17]. In the energy range above 538 eV, the absorption peaks [B_{4-6} in Fig. 1(b)] are due to the O 2p states mixed with Zr 5s states. Increasing the Fe atomic concentration, the peaks broaden, and for $x = 24\%$ at., it is no more possible to resolve the fine structure. For this Fe concentration, a significant decrease in intensity of the sharp B_3 peak occurs. This can be tentatively ascribed to the formation of oxygen vacancies which can affect the surrounding shell of oxygen atoms. In fact, considering that Fe can have at most a 3+ valence and substitutes a 4+ Zr atom, oxygen vacancies reasonably form for charge compensation upon increasing Fe doping. Moreover, at energy lower than 530 eV and for Fe atomic concentration higher than 6%, a pre-edge B_1 peak is present whose relative intensity increases with increasing the Fe content. This pre-edge peak can be ascribed to O 2p states hybridized with the Fe 3d states [14,15]. This issue will be extensively discussed later in the theoretical part of this work.

As for the XAS spectra recorded at the Fe $L_{2,3}$-edge [Fig. 1(c)], the well defined peaks C_{1-4} indicate the presence of localized states, their relative intensities suggest that the valence state of Fe is probably a mixture of 2+ and 3+ [18,19]. The pre-edge peak C_1 increases in sharpness with increasing the Fe atomic concentration, suggesting an increase of the 3+ sites. The predominance of 3+ is in agreement with the formation of a large amount of oxygen vacancies for charge neutrality. No significant differences were found between the XAS spectra measured at room temperature (RT) and at lower temperature (LT) ∽30 K. XMCD measurements show no evidence of ferromagnetic (FM) order for all the analyzed samples both at RT and LT ∽30 K. Moreover, neither performing XMCD with an applied field nor performing XMCD after field cooling, we were able to detect signs of paramagnetic behavior, thus suggesting the AFM order as the favorite phase of the system.

From the above results, the most significant change in the shape of XANES spectra is observed at the O K-edge, especially in the pre-edge region where the pre-edge peak appears and increases with Fe atomic concentration. This behavior could help us to elucidate the enhancement of AFM interactions with the increase of Fe atomic concentration and investigate the origin of this pre-edge peak. For this reason, the theoretical part of this work is focused on the O K-edge spectra.

III. COMPUTATIONAL APPROACH

First-principles calculations have been performed with QUANTUM ESPRESSO code [20] using a plane-waves basis set in the pseudopotential approach and periodic boundary conditions. We used the ultrasoft pseudopotentials and the generalized gradient approximation (GGA) in the parametrization of Perdew, Burke, and Ernzerhof (PBE) [21] for the exchange-correlation functional.

A. Structural relaxation

A tetragonal supercell of zirconia containing 32 ZrO_2 units (96 atoms) has been used to reproduce experimental data. Each Zr^{4+} cation in the supercell is surrounded by 8 O^{2-} anions divided in two shells [22]. Four oxygen atoms with a shorter-length Zr-O bond forming a flattened tetrahedron constitute the first oxygen shell and four other oxygen atoms with a longer-length Zr-O bond forming an elongated tetrahedron constitute the second shell. We performed simulations for different Fe atomic concentrations, namely, 6.25%, 12.5%, and 25%, obtained by substituting, respectively, two, four, and eight Zr atoms with an equivalent number of Fe atoms in tetrahedral coordination. The Fe atoms were placed at the substitutional Zr sites and kept as far as possible from each other to mimic uniform doping. As shown previously in Refs. [6–8], substituting Zr^{4+} by Fe^{3+} cations in the pure zirconia induces oxygen vacancies in order to maintain charge neutrality. The ratio between oxygen vacancies and Fe impurities is 0.5, i.e., one vacancy for each Fe pair as required for Fe^{3+} oxidation state. This computational model is capable to reproduce structural and electronic properties of ZrO_2:Fe at different doping concentrations as proved in Refs. [6–8] (see also Ref. [23] where yttrium, a substitutional impurity with the same valence of Fe is considered). The oxygen vacancies induce a disorder in the system, thus the whole structure has been relaxed by an *ab initio* energy minimization calculation. This structural relaxation is performed with the basis set consisting of plane waves up to a maximal kinetic energy of 35 and 400 Ry to represent the Kohn-Sham (KS) orbitals and the charge density, respectively, while the Brillouin zone is sampled using a Monkhorst-Pack grid $2 \times 2 \times 2$. The convergence parameters are 10^{-8} Ry on the total energy of self consistent cycle and 10^{-3} Ry/Bohr on the forces for the atomic relaxation. The spin polarization has been taken into account, and we found that the antiferromagnetic coupling is the most stable configuration in comparison to the ferromagnetic one. We present in Fig. 2 the relaxed structures of ZrO_2:Fe for different Fe atomic concentrations used in our simulations. In this figure, one can see that Fe atoms remain in tetrahedral coordination with the surrounding oxygen atoms.

B. XANES calculation

XANES spectra are computed using the XSPECTRA package [24] included in QUANTUM ESPRESSO. Within DFT approach, the x-ray absorption cross-section is expressed in terms of a transition operator coupling the initial and the final states, which are solutions of KS equations. In the case of K-edge, the initial state is a core 1s orbital calculated from an isolated absorbing atom in the absence of a core hole, while the final state is obtained self-consistently through the resolution of KS equations for the whole system including core hole effects in the pseudopotential of the absorbing atom [24].

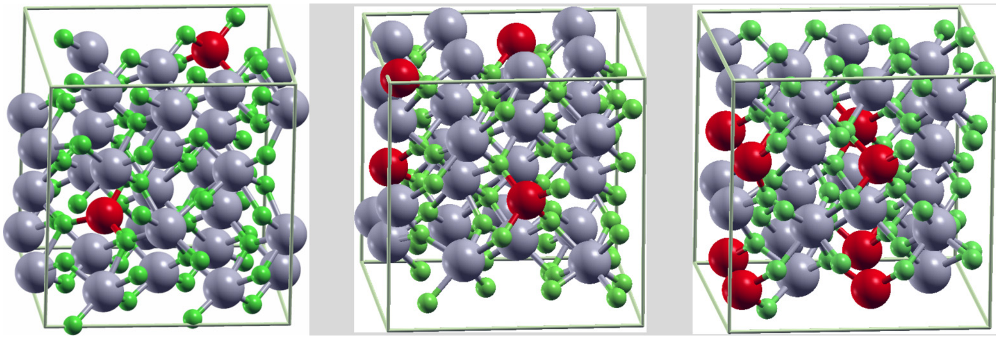

FIG. 2. (Color online) Relaxed structures of ZrO_2:Fe for different Fe atomic concentrations namely 6.25%, 12.5%, and 25%, respectively, from left to right. Zr, O, and Fe atoms are, respectively, in gray, green, and red colors.

Within the pseudopotential approach, the final all-electron wave function is reconstructed from the pseudowave function by means of projector augmented wave (PAW) method [25]. The experimental sample used in this work has no preferential orientation, hence, the isotropic cross section has been considered ideal to reproduce the experimental XANES spectra. For a general symmetry, the isotropic electric dipole cross-section is obtained by a linear combination of three cross sections calculated along three perpendicular directions of polarization namely $\sigma(0,0) = \frac{1}{3}(\sigma_{xx} + \sigma_{yy} + \sigma_{zz})$ [26]. In the practice, the cross-section is calculated as follows: first, the charge density is obtained through a DFT calculation with a 1s core-hole on the absorbing oxygen atom, and the cross-section is finally calculated for a given polarization direction using the Lanczos method and the continued fraction [27]. This approach does not require an explicit calculation of empty states and is very fast since only the charge density is needed [24]. The supercell consisting of 96 atoms (few less when the doping concentration increases) is assumed to be large enough to avoid the interaction between periodic images of the absorbing atom. For convergence reasons, the cutoff energies of KS orbitals and the charge density are increased, respectively, to 50 and 500 Ry while the k-point mesh is kept unchanged. A Lorentzian convolution with a variable broadening parameter γ has been applied in the continued fraction. For this purpose, we used $\gamma = 0.3$ eV up to 1.5 eV photon energy and $\gamma = 0.8$ eV from 10 eV photon energy, with a linear variation in the intermediate photon range.

C. First-principles results

We performed simulations for different Fe atomic concentrations by starting with pure zirconia, i.e., $x = 0\%$. In this case, the XANES spectrum is needed only for one oxygen site since all the oxygen atoms are equivalent. The resulting spectrum is presented in Fig. 3(a) where the Fermi level is considered as zero energy in the plot.

To investigate the effect of Fe doping on pure zirconia, we start with the lowest Fe atomic concentration ($x = 6.25\%$). At this concentration, the average distance between Fe impurities is large enough ($d \sim 9$ Å) to minimize the interactions between two Fe atoms. This allows us to elucidate the effect of one Fe atom on its local environment (nearest oxygen atoms) with a minimal influence from Fe neighbors. The disorder caused by the substitution of Zr atoms with the Fe ones implies that the O K-edge XANES spectrum results from the average of the contributions coming from all the oxygen atoms in the supercell. The resulting O K-edge spectrum [Fig. 3(a)] shows a shift of about -1.5 eV of the whole spectrum and a change in the intensities of the peaks in comparison with the case of pure zirconia. The most marked difference between the two spectra occurs in the pre-edge region, where a pre-edge peak appears in the energy range between 0 and 1.43 eV.

For a deep understanding of the origin of this pre-edge peak, we consider one absorbing oxygen atom located in the first shell around one iron atom with spin-down polarization. For these two atoms, we have plotted the Löwdin projected density of states (PDOS) presented in Fig. 3(c). The PDOS analysis shows a strong hybridization between the unoccupied Fe $3d$ up-spin states and $2p$ up-spin states of the absorbing atom. Taking into account the spin-polarization, the O K-edge spectrum can be separated in spin-up and spin-down polarizations. The spin-resolved dipolar spectrum is presented in Fig. 3(b) and shows that the pre-edge peak is mainly due to the contribution of the up-spin polarized component of the spectrum. Thus the pre-edge peak is due to dipole transitions from O $1s$ to O $2p$ up-spin states hybridized with the unoccupied Fe $3d$ up-spin states. A similar conclusion has been done previously in the case of perovskite- alloy LaBO$_3$:Ga ($B =$ Fe, Mn) by an *ab initio* method based on multiple scattering theory using cluster model [28]. The above results suggest that Fe^{3+} with a valence orbital $3d^5$ in tetrahedral coordination is in high spin polarization with an electron configuration $e_g^2 t_{2g}^3$ according to ligand field theory [29–31]. In this case, e_g and t_{2g} orbitals participate together to the transitions that occur in the pre-edge region [see Figs. 3(b) and 3(c)].

Moreover, our theoretical results reveal the increase of the pre-edge peak when the Fe atomic concentration increases [see Fig. 4(a)]. This behavior is in perfect agreement with our experimental results presented in Fig. 1(b). Note that the absorption peak B_2 in Fig. 4(a) for each Fe concentration is set to 531.18 eV in order to make a direct comparison with the experimental results. To have a clear picture of this effect, let first consider three oxygen atoms located, respectively, in the first, second, and third shell around one Fe atom in the case of $x = 6.25\%$. We observe that the pre-edge peak is maximum when the oxygen atom is located in the first shell, almost negligible in the second, and disappears completely in the third shell where the spectrum feature is close to the case of pure

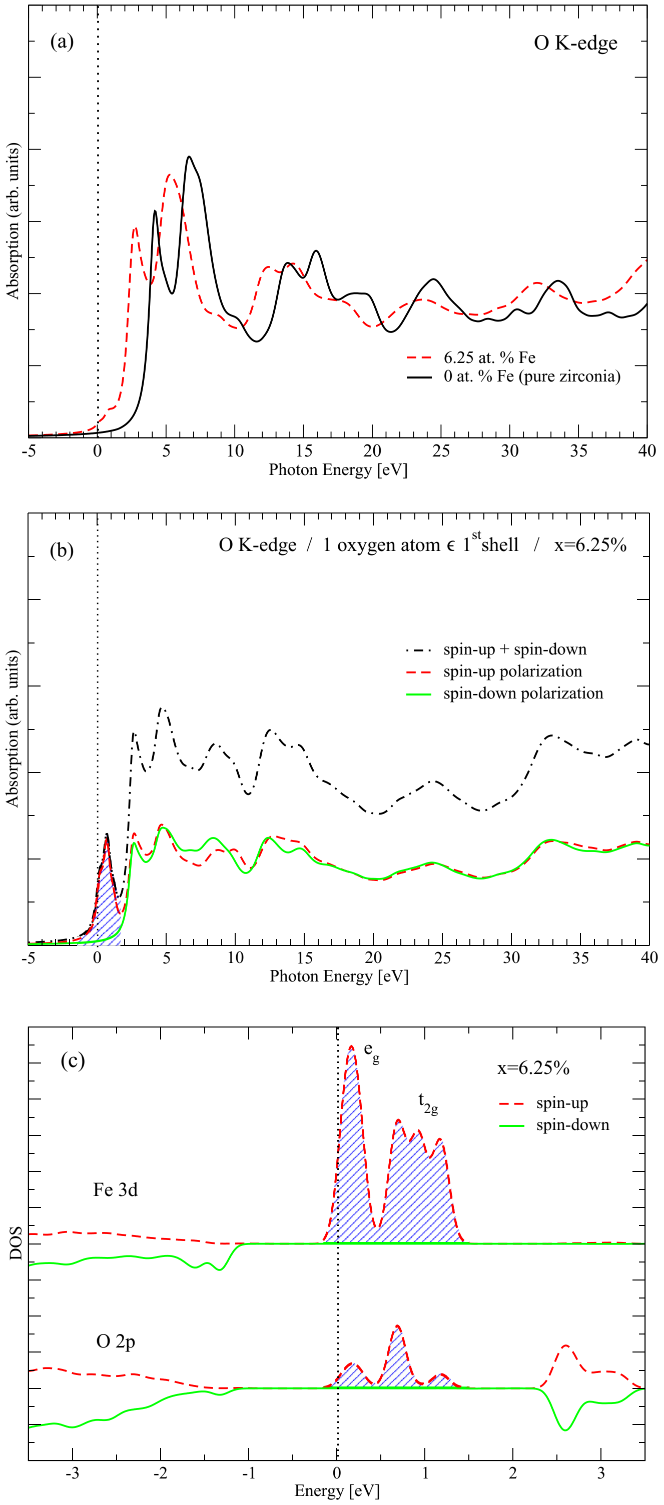

FIG. 3. (Color online) (a) Calculated O K-edge XANES spectra in iron-doped zirconia (ZrO$_2$:Fe) at $x = 6.25\%$ and in pure zirconia. Note the presence of pre-edge peak and energy shift for the case of ZrO$_2$:Fe. (b) Spin-polarization dependence of the O K-edge XANES spectrum of one oxygen atom located in the first shell around one spin-down polarized Fe atom. (c) Löwdin DOS projected, respectively, on the 2p orbital of the absorbing oxygen atom and 3d orbital of the nearest Fe. The hatched areas in (c) show the PDOS peaks responsible for the pre-edge peak marked as hatched area in (b).

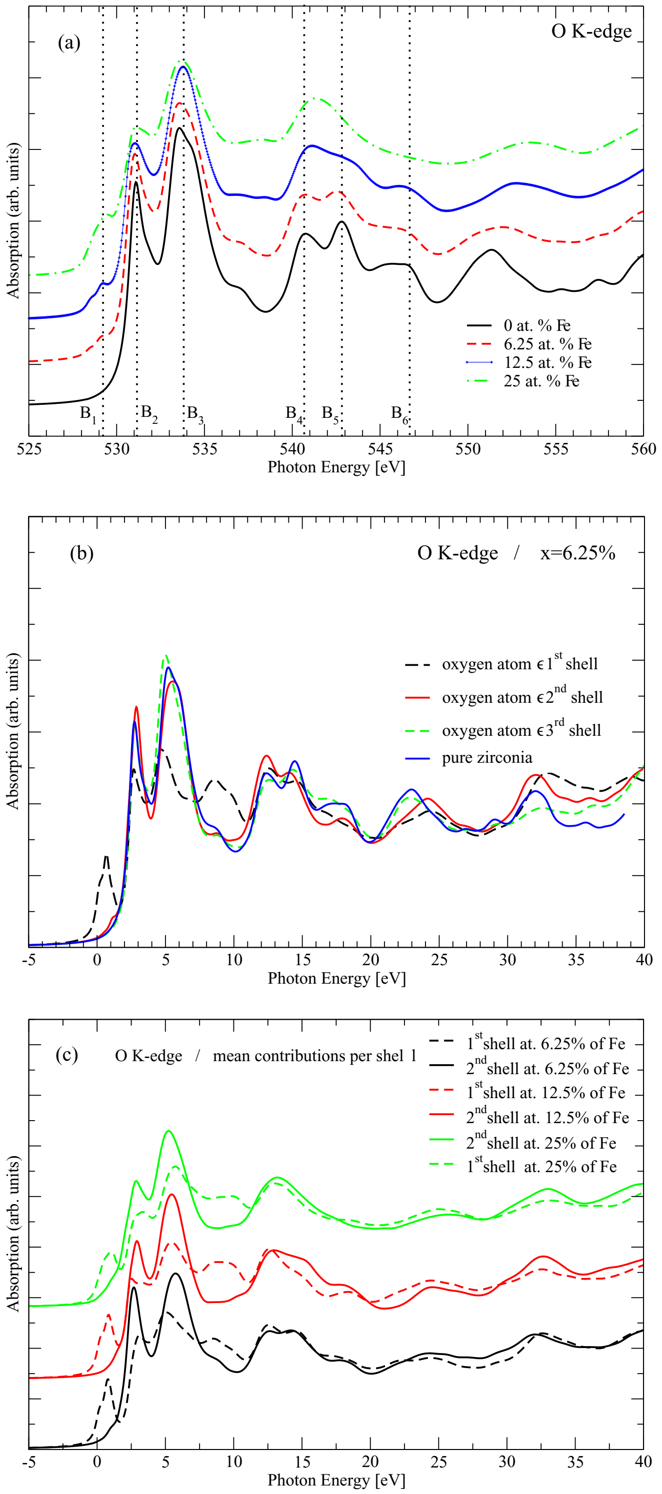

FIG. 4. (Color online) (a) Evolution of O K-edge XANES spectrum with respect to iron concentration. The absorption peaks B$_2$ are set to 531.18 eV in order to make a direct comparison with the experimental results. (b) shows that the pre-edge peak originates mainly from the first oxygen shell around the iron atom and a small contribution coming from the second oxygen shell. (c) The mean contributions of the two first oxygen shells in the O K-edge spectra.

TABLE I. Total numbers of different types of atoms in the simulation supercells (n_O, n_{Fe}, and n_{Zr}) for each doping concentration and the corresponding numbers of oxygen atoms per shell contributing in the O K-edge XANES spectra.

Fe %	n_O	n_{Fe}	n_{Zr}	1st shell	2nd shell	shells > 2
6.25%	63 O	2 Fe	30 Zr	8 O	7 O	48 O
12.5%	62 O	4 Fe	28 Zr	16 O	14 O	32 O
25%	60 O	8 Fe	24 Zr	32 O	28 O	0 O

zirconia [see Fig. 4(b)]. This behavior shows that the effect of Fe atoms on the pre-edge region is mainly localized in the first oxygen shell and disappears as one moves far from it.

Let now consider two groups of absorbing atoms, the first one constituted by the oxygen atoms located in the first shell and the second one with the oxygen atoms located in the second shell, in the cases of $x = 6.25\%$, 12.5%, and 25%. For each of these three Fe atomic concentrations, we present in Fig. 4(c) the mean contributions of the two oxygen shells in the O K-edge XANES spectrum. In spite of the difference in the number of oxygen atoms located in the two first shells of these three concentrations (see Table I), their mean contributions in the pre-edge region are quite similar.

From the above observations, it is clear that at high doping concentration, the intensity of the pre-edge peak is mostly dictated by the first oxygen shell, while the low doping concentration is mostly affected by the shells of order higher than two, which lower the intensity of the pre-edge peak in the average spectrum. Thus the increase of the pre-edge peak with increasing Fe atomic concentration is related to the increase of oxygen atoms located in the first shell (nearest neighbours to Fe atoms) associated to the decrease of oxygen atoms located in the shells of order higher than two (see Table I), which contribute less on the pre-edge peak, since the O K-edge spectrum for each doping concentration is calculated by averaging the contributions of all the oxygen atoms in the system. The agreement between theoretical and experimental XANES data provides further assessment of the validity of the structural model used in the present and previous [6–8] simulations. According to this simulation model, the increase of Fe atomic concentration increases the unpaired Fe $3d$ states and oxygen vacancies in the sample, which have as a consequence the improvement of AFM interaction between Fe^{3+} ions as observed experimentally by Yu *et al.* [4] in the case of ZrO_2:Fe nanoparticles prepared by a coprecipitation method.

In this work, iron atoms are considered in oxidation state Fe^{3+}. However, we expect that the results we found concerning the origin of the pre-edge peak and its increasing with Fe atomic concentration should be qualitatively valid in the case of Fe^{2+} since this latter also contains $3d$ unoccupied states.

IV. CONCLUSION

We have investigated the Fe doping effect on zirconia films by mean of XANES spectroscopy both experimentally and theoretically. Considering that Fe atoms are uniformly distributed in the sample, our theoretical investigations revealed the formation of an AFM ground state in agreement with experimental results. The pre-edge peak has not been observed on the K-edge of oxygen atoms belonging to the shells of order higher than two, which shows its local character. We demonstrated that the increase of this O K-pre-edge peak with Fe atomic concentration is due to the increase of percentage of atoms that are near neighbors to Fe atoms. This increase of Fe $3d$ unpaired states (i.e., spin polarized) in the system and the increase of oxygen vacancies (at a rate of 0.5 oxygen vacancy per Fe atom according to the structural model that we used) can be responsible for the magnetic behavior of ZrO_2:Fe.

ACKNOWLEDGMENTS

We acknowledge the Fondazione Cariplo for funding through the OSEA project (No. 2009-2552), CINECA-Rome (ex CASPUR) for computational resources provided under the project MOSE, APE beamline staff for technical support, G. Panaccione for helpful discussions, R. Colnaghi and M. Alia for technical support.

[1] V. Barthem, C. Colin, H. Mayaffre, M.-H. Julien, and D. Givord, Nat. Commun. **4**, 2892 (2013).

[2] A. B. Shick, S. Khmelevskyi, O. N. Mryasov, J. Wunderlich, and T. Jungwirth, Phys. Rev. B **81**, 212409 (2010).

[3] N. H. Hong, M. B. Kanoun, S. Goumri-Said, J.-H. Song, E. Chikoidze, Y. Dumont, A. Ruyter, and M. Kurisu, J. Phys.: Condens. Matter **25**, 436003 (2013).

[4] J. Yu, L. Duan, Y. Wang, and G. Rao, Physica B: Condens. Matter **403**, 4264 (2008).

[5] A. Lamperti, E. Cianci, R. Ciprian, D. Sangalli, and A. Debernardi, Thin Solid Films **533**, 83 (2013).

[6] A. Debernardi, D. Sangalli, A. Lamperti, E. Cianci, P. Lupo, F. Casoli, F. Albertini, L. Nasi, R. Ciprian, and P. Torelli, J. Appl. Phys. **115**, 17D718 (2014).

[7] D. Sangalli, A. Lamperti, E. Cianci, R. Ciprian, M. Perego, and A. Debernardi, Phys. Rev. B **87**, 085206 (2013).

[8] D. Sangalli, E. Cianci, A. Lamperti, R. Ciprian, F. Albertini, F. Casoli, P. Lupo, L. Nasi, M. Campanini, and A. Debernardi, Eur. Phys. J. B **86**, 211 (2013).

[9] G. Panaccione, I. Vobornik, J. Fujii, D. Krizmancic, E. Annese, L. Giovanelli, F. Maccherozzi, F. Salvador, A. De Luisa, D. Benedetti, A. Gruden, P. Bertoch, F. Polack, D. Cocco, G. Sostero, B. Diviacco, M. Hochstrasser, U. Maier, D. Pescia, C. H. Back, T. Greber, J. Osterwalder, M. Galaktionov, M. Sancrotti, and G. Rossi, Rev. Sci. Instrum. **80**, 043105 (2009).

[10] G. Lucovsky, G. B. Rayner, Y. Zhang, C. C. Fulton, R. J. Nemanich, G. Appel, H. Ade, and J. L. Whitten, Appl. Surf. Sci. **212-213**, 563 (2003).

[11] A. Kikas, J. Aarik, V. Kisand, K. Kooser, T. Kmbre, H. Mndar, T. Uustare, R. Rammula, V. Sammelselg, and I. Martinson, J. Electron Spectrosc. Relat. Phenom. **156–158**, 303 (2007).

[12] A. P. Singh, R. Kumar, P. Thakur, N. Brookes, K. Chae, and W. Choi, J. Phys.: Condens. Matter **21**, 185005 (2009).

[13] P. G. Karlsson, L. Johansson, J. H. Richter, C. Virojanadara, J. Blomquist, P. Uvdal, and A. Sandell, Surf. Sci. **601**, 2390 (2007).

[14] P. Satyarthi, S. Ghosh, B. Pandey, P. Kumar, C. Chen, C. Dong, W. Pong, D. Kanjilal, K. Asokan, and P. Srivastava, J. Appl. Phys. **113**, 183708 (2013).

[15] T. Higuchi, K. Kobayashi, S. Yamaguchi, A. Fukushima, S. Shin, and T. Tsukamoto, Jpn. J. Appl. Phys., Part 1. **42**, L941 (2003).

[16] L. Soriano, M. Abbate, J. Fuggle, M. Jimenez, J. Sanz, C. Mythen, and H. Padmore, Solid State Commun. **87**, 699 (1993).

[17] D.-Y. Cho, H.-S. Jung, J. H. Kim, and C. S. Hwang, Appl. Phys. Lett. **97**, 141905 (2010).

[18] T. J. Regan, H. Ohldag, C. Stamm, F. Nolting, J. Lüning, J. Stöhr, and R. L. White, Phys. Rev. B **64**, 214422 (2001).

[19] S. Zhou, K. Potzger, G. Talut, H. Reuther, K. Kuepper, J. Grenzer, Q. Xu, A. Mücklich, M. Helm, J. Fassbender *et al.*, J. Phys. D: Appl. Phys. **41**, 105011 (2008).

[20] P. Giannozzi, S. Baroni, N. Bonini, M. Calandra, R. Car, C. Cavazzoni, D. Ceresoli, G. L. Chiarotti, M. Cococcioni, I. Dabo *et al.*, J. Phys.: Condens. Matter **21**, 395502 (2009).

[21] J. P. Perdew, K. Burke, and M. Ernzerhof, Phys. Rev. Lett. **77**, 3865 (1996).

[22] D. Wang, Y. Guo, K. Liang, and K. Tao, Sci. China, Ser. A: Math., Phys., Astron. **42**, 80 (1999).

[23] D. Sangalli and A. Debernardi, Phys. Rev. B **84**, 214113 (2011).

[24] C. Gougoussis, M. Calandra, A. P. Seitsonen, and F. Mauri, Phys. Rev. B **80**, 075102 (2009).

[25] P. E. Blöchl, Phys. Rev. B **50**, 17953 (1994).

[26] C. Brouder, J. Phys.: Condens. Matter **2**, 701 (1990).

[27] M. Taillefumier, D. Cabaret, A.-M. Flank, and F. Mauri, Phys. Rev. B **66**, 195107 (2002).

[28] S. Lafuerza, G. Subias, J. Garcia, S. Di Matteo, J. Blasco, V. Cuartero, and C. R. Natoli, J. Phys.: Condens. Matter **23**, 325601 (2011).

[29] C. J. Ballhausen, *Introduction to Ligand-Field Theory* (McGraw-Hill, New York, 1962).

[30] J. Griffith and L. Orgel, Q. Rev. Chem. Soc. **11**, 381 (1957).

[31] B. N. Figgis, in *Comprehensive Coordination Chemistry*, edited by G. Wilkinson (Pergamon, Oxford, 1987), p. 243.